A versatile method for the selective core-crosslinking of hyaluronic acid nanogels via ketone-hydrazide chemistry: from chemical characterization to in vivo biodistribution

Francielle Pelegrin Garcia, Marlène Rippe, Mychelle Vianna P. Companhoni, Talitha Fernandes Stefanello, Benoit Louage, Simon van Herck, Lucie Sancey, Jean-Luc Coll, Bruno G de Geest, Celso Vataru Nakamura, et al.

Biomaterials Science

A versatile method for the selective core-crosslinking of hyaluronic acid-based nanogels via ketone-hydrazide chemistry: from chemical characterization to *in vivo* biodistribution

Francielle Pelegrin Garcia [a,b], Marlene Rippe [a], Mychelle Vianna [b], Talitha Fernandes Stefanello [a,b], Benoit Louage[c], Simon Van Herck[c], Lucie Sancey[d], Jean-Luc Coll[d], Bruno G. De Geest[c], Celso Vataru Nakamura [b], Rachel Auzély-Velty*[a]

The development of biopolymer-based nanogels has gained particular interest to achieve successful delivery of therapeutics for the treatment of various diseases, such as cancer, infection and diabetes. Herein, we report a new and simple methodology for the covalent stabilization of self-assembled gel nanoparticles based on hyaluronic acid (HA) modified with a thermoresponsive ketone-functional copolymer. This relies on the selective formation of hydrazone crosslinks with bishydrazides within the globular domains of the copolymer chains formed above the cloud point temperature. This approach allows tuning the crosslinking density by varying the dihydrazide crosslinker to ketone molar ratio. The size distributions and morphology of the nanogels were assessed using dynamic light scattering (DLS), cryo-transmission and scannning electron microscopy. *In vitro* cellular uptake in several cancer cells and *in vivo* biodistribution of the nanogels in different mouse tumor models were then explored to assess the effectiveness of this crosslinking strategy. The data from these experiments show prolonged blood circulation, longer than 24 hours, for the crosslinked nanogels and high tumor accumulation.

Introduction

Self-assembled gel nanoparticles (also called nanogels) made of hydrophobically modified biopolymers have attracted growing interest for drug delivery to tumors as these systems combine the advantages of hydrogels with nanoscale formulations.[1-5] Their size can be easily tuned from tens to several hundreds of nanometer, their inner network comprising hydrophobic domains can be used to incorporate poorly water-soluble drugs and their hydrophilic shell can be exploited to control their biological fate and targeting ability. However, one practical challenge with such carrier systems is their tendency to disassemble in the bloodstream because of the large dilution volume and/or interactions with serum proteins.[6] These negative events reduce the efficiency of tumor-targeted drug delivery *via* the enhanced permeability and retention (EPR) effect[7, 8]. To stabilize the nanocarriers, strategies of shell or core-crosslinking have been employed.[9-13] Among these methods, crosslinking the hydrophobic domains in the nanogel core rather than the hydrophilic shell has the advantage of preserving the intrinsic properties of the biopolymer forming the hydrophilic shell.

In this study, we aimed to establish a simple and reliable method for the synthesis of core-crosslinked nanogels based on hyaluronic acid (HA) for improved nanogel stability in view of *in vivo* tumor-targeting. HA, a polysaccharide which is a main component of the extracellular matrix, was selected as hydrophilic component due its biocompatibility, biodegradability and the existence of various functional groups that are accessible for chemical modification.[14] Despite intensive research on self-assembled nanoparticles based on hydrophobically modified HA for targeted anti-cancer drug delivery,[14-16] core-crosslinking has only recently been explored to address the issue of nanoparticle stability under diluted serum-rich conditions. In reported examples, the hydrophobic core of HA-based nanoparticles was crosslinked by disulfide- or photo-mediated crosslinking. Here, we present a new approach based on acylhydrazone chemistry allowing to tailor the density of crosslinking.[17-21] Key to our strategy is the chemical modification of HA by a temperature-responsive keto-functional polymer which can be efficiently crosslinked by bifunctional hydrazides in aqueous medium (Scheme 1). Keto-functionalized polymers have been demonstrated to be useful reactive scaffolds for the design of complex macromolecular architectures and for the conjugation of fragile biomolecules since they can be modified easily and in high yield.[22-27] Herein, the keto-polymer plays a dual role: i) in inducing hydrophobically-driven self-assembly of modified HA into nanogels due to its dehydration upon heating, and ii) in stabilizing the nanogel structure through crosslinking by hydrazone bond formation between ketones and hydrazides. We further investigated cellular uptake of the nanogels in several cancer cells and their *in vivo* biodistribution to assess their tumor targeting potential.

Materials and methods

Materials

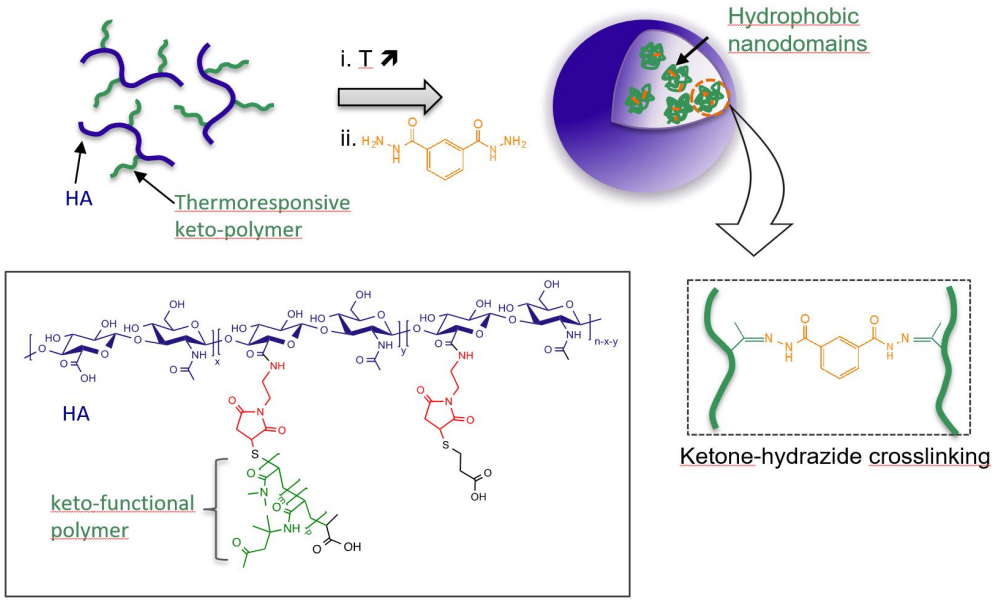

Scheme 1. Formation of hyaluronic acid-based nanogels by temperature-induced self-assembly and their covalent crosslinking by hydrazone bond formation within the hydrophobic domains of the grafted copolymer chains.

Hyaluronic acid (M_w = 40 kg/mol) was purchased from Lifecore (USA). Diacetone acrylamide (DAAM), *N,N*-dimethylacrylamide (DMA), 2,2-azobis(2-methylpropionitrile) (AIBN), phosphate buffer saline (PBS, pH 7.4), Tris-(2-carboxyethyl) phosphine hydrochloride (TCEP), mercaptopropionic acid (MPA), 3-(4,5-dimethylthiazol-2-yl)-2,5-diphenyltetrazolium bromide (MTT) and 4-(4,6-dimethoxy-1,3,5-triazin-2-yl)-4-methylmorpholinium chloride (DMTMM), isophtalic acid dihydrazide (IDH), hyaluronidase (type IV from bovine testes) were purchased from Sigma-Aldrich-Fluka (France). Aminoethylmaleimide hydrochloride was purchased from Aokchem. *N*-hydroxysulfosuccinimide sodium salt (sulfo-NHS) was obtained from Chemrio. *N*-(3-dimethylaminopropyl)-*N'*-ethylcarbodiimide hydrochloride (EDC) was purchased from Acros Organics. Dulbecco's Modified Eagle Medium (DMEM), L-glutamine, sodium pyruvate, fetal bovine serum (FBS), penicillin and streptomycin were provided by Gibco. Cyanine 5.5-amine (Cy5.5-amine) was purchased from Lumiprobe. All chemicals were used without any further purification. The positively charged resin, diethylaminoethyl cellulose (DEAE) was purchased from GE Healthcare Life Science. 2-(Butylthiocarbonothioylthio)propanoic acid (PABTC) was synthesized as previously reported.[28] The water used in all experiments was purified by an Elga Purelab purification system, with a resistivity of 18.2 MΩ cm.

Analytical techniques

^{1}H NMR spectra were recorded at 25 °C using a Bruker AVANCE III HD spectrometer operating at 400 MHz. Deuterium oxide (D_2O) and dimethysulfoxide-d6 (DMSO-d6) were obtained from SDS (Vitry, France). All spectra were recorded by applying a 45° tip angle for the excitation pulse, and a 10 s recycle delay. Chemical shifts (δ in ppm) are given relative to external tetramethylsilane (TMS = 0 ppm) and calibration was performed using the signal of the residual protons of the solvent as a secondary reference. The number-average molar mass (M_n), the weight-average molar mass (M_w) and the dispersity ($Đ$) of poly(DAAM-co-DMA) were determined by size exclusion chromatography (SEC) in dimethylformamide containing 50 mM $NaNO_3$. Measurements were done on a GPC system equipped with a Waters model 515 pump, a refractive Index Detector RI 2000 from Schambeck SFD GmbH and a light scattering detector (MALLS) from Wyatt (USA); Samples were recorded at 30 °C and at a flow rate of 1 mL/min. The cloud point temperature (T_{cp}) of poly(DAAM-co-DMA) was determined by UV-vis turbidity measurements (λ = 500 nm) performed on a Varian Cary 50 Scan. The samples were prepared at room temperature in PBS (1 and 3 g/L), after which the sample was placed in the instrument. The light transmittance was measured during at least two controlled cooling/heating cycles from 15 °C to 35 °C using a 2 °C interval. T_{CP} was considered to be the temperature at which the light transmittance was 50 % of that obtained for the same sample at 15 °C. The critical aggregation temperature (CAT) of HA-m-poly(DAAM-co-DMA) in aqueous solution was assessed by static light scattering (SLS) using an ALV 5000 device (ALV-Langen, Germany) equipped with a red helium-neon laser at a wavelength of 632.8 nm. A solution of HA-m-poly(DAAM-co-DMA) in PBS at a concentration of 0.5 g/L was filtered through a 1.2 µm polycarbonate filter and heated from 10 to 50 °C using a 5 °C interval. The light scattering intensity (LSI) was measured at 90° angle for 60 s. The CAT, defined as the temperature at the inflection point of the plotted curve, was found to be 32 °C. The size and size distribution of nanogels were

measured by dynamic light scattering (DLS) using a Zetasizer NanoZS Malvern Instruments apparatus operating with a HeNe laser at 173°. The hydrodynamic diameters were calculated from diffusion coefficients using the Stokes-Einstein equation. All correlogram analyses were performed with software supplied by the manufacturer. All the measurements were performed in PBS (pH 7.4, [NaCl] = 0.15 M).

Synthesis of copolymer poly(DAAM-co-DMA)

DMA (0.515 mL, 5 mmol) and DAAM (1.69 g, 10 mmol), the RAFT agent PABTC (35.7 mg, 0.2 mmol) and AIBN (5 mg, 0.03 mmol) in 7 mL anhydrous dioxane were placed into a Schlenk tube under nitrogen. After 5 freeze-pump-thaw cycles for the deoxygenation of the solution, the resulting solution was immersed in a thermostated oil bath at 75 °C and left to react for 3 h. The reaction was quenched by cooling and exposure to oxygen. The resulting polymer was precipitated in cold hexane. The precipitate was dissolved in acetone and the copolymer was precipitated again in hexane. This step was repeated 3 times to give 1.85 g of pure poly($DAAM_{57}$-co-DMA_{33}). Samples taken before and during the polymerization were analyzed by ^{1}H NMR to determine monomers conversion. The M_n, M_w and $Đ$ values of the copolymer were determined by SEC in DMF.

Synthesis of HA-m-poly(DAAM-co-DMA)

Prior to the coupling reaction with HA-maleimide, the poly(DAAM-co-DMA) copolymer was subjected to aminolysis using *n*-butylamine, to convert the RAFT end-group to a thiol. Briefly, the copolymer (0.370 g, 0.225 mmol) was solubilized in tetrahydrofuran (10 mL) and *n*-butylamine (4 mL, 0.04 mol) was added. After 5 min under stirring, the reaction mixture was concentrated under reduced pressure, resulting in a waxy liquid that was solubilized in THF. The copolymer was recovered by precipitation in cyclohexane and dried under vacuum at 45 °C to obtain a white powder. Next, the thiol-capped copolymer (0.360 g, 0.0218 mmol) was solubilized in 10 mL of water/ethanol (3:2, v/v) and TCEP (0.0063 g, 0.0218 mmol) was added. After 30 min of stirring at 4 °C under nitrogen atmosphere, the copolymer solution was added to a solution of HA-maleimide (0.124 mmol) in 40 mL of PBS/ethanol (3:2, v/v), to perform the coupling reaction via Michael addition, as previously described[29].

To prepare the HA-maleimide derivative, HA (0.065 g, 0.162 mmol) was dissolved in 31.5 mL of a water/ethanol mixture (2:1,v/v) and sodium chloride (0.257 g, 7.24 mmol) was added. Next, aminoethylmaleimide hydrochloride (0.068 g, 0.385 mmol), sulfo-NHS (0.070 g, 0.324 mmol) and EDC (0.124 g, 0.65 mmol) were added and the pH of the solution was maintained between 4.5 and 5 until no further change of pH was observed (≈ 4 h). The resulting product was purified by diafiltration using a membrane Amicon Ultracel MWCO 10 KDa and recovered in pure water (24 mL). Then, PBS 0.1 M (10-fold concentrated) (2.4 mL) was added, followed by immediately adjusting the pH to 4.5. Finally, the copolymer solution was added to the HA-maleimide solution (0.050 g in 18.5 mL, 0.124 mmol) and the reaction mixture was stirred at 4 °C for 4 h. The remaining maleimide units were then converted to carboxylic acid derivatives by addition of excess MPA (42.5 µL, 0.49 mmol). After stirring for 6 h, the HA-poly(DMA-co-DAAM) derivative was purified via a batch ion exchange process using DEAE Sepharose CL-6B as a weak-anion exchanger. Briefly, DEAE resin (20 mL), stored in a solution of ethanol 30 %, was washed three times with ultrapure water at 4 °C (3 × 20 mL, contact times of 10 min). Excess liquid was removed by centrifugation (10,000 rpm, 10 min) at 4° C. Then, the resin was activated by successive washes with a 0.5 M NaCl aqueous solution (20 mL), a 1 M NaCl aqueous solution (20 mL) and finally, four times with ultrapure water (4 × 20 mL). The HA-poly(DMA-co-DAAM) derivative was then added to the resin in a conical tube and allowed to interact with the resin overnight at 4°C under stirring with an orbital shaker. Then, the HA-derivative bound to the resin was subjected to four washes with ultrapure water (4 × 20 mL) to remove non-grafted copolymer. Finally, the HA-derivative was eluted with a 1 M NaCl aqueous solution (4 × 10 mL). After filtration of the solutions of the recovered HA derivative through a Buchner funnel containing a porous glass filter plate (porosity 4), the solution was dialyzed against deionized water using a dialysis membrane MWCO 100 kDa for 48 h. The product was recovered by freeze-drying as a white powder.

Determination of the poly(DAAM-co-DMA) content in HA-m-poly(DAAM-co-DMA) samples by the carbazole reaction

The degree of substitution (DS), defined as the average number of copolymer units per repeating disaccharide unit, was indirectly determined by reaction of D-glucuronic acid units of HA with carbazole[30]. Briefly, 800 µL of 25 mM sodium tetraborate solution in sulfuric acid was added to an aqueous solution of HA-m-poly(DAAM-co-DMA) (200 µL) at a concentration of 0.34 g/L. After heating at 100 °C for 10 min, the solution was cooled at room temperature for 15 min, and then a solution of carbazole (200 µL) in absolute ethanol 0.125 % (m/v) was added. The sample was heated again at 100 °C for 10 min and its absorbance was determined by spectrophotometry at 530 nm. The HA concentration was calculated from a calibration curve (0.050 to 0.250 g/L), which allowed the indirect determination of the copolymer amount in the HA-m-poly(DAAM-co-DMA) sample.

Nanogel crosslinking

To a solution of HA-m-poly(DMA-co-DAAM) (0.005 g, 0.0026 mmol) with a DS of 0.1 at a concentration of 1 g/L in PBS (pH 7.4) at room temperature, a solution of isophtalic acid dihydrazide (IDH) in DMSO (0.073 g/mL) was added under stirring. The volume of the IDH solution (20, 40 and 60 µL) was varied to obtain IDH/ketone molar ratios of 0.5, 1.0 and 1.5, respectively. Next, the

temperature of the solution was increased to 40 °C. After stirring at 40 °C for 24 h, the nanogels suspension was transferred into a dialysis bag (MWCO = 6-8 kDa) and dialyzed against deionized water for 48 h. The core cross-linked nanogels were recovered by freeze-drying.

Labeling of crosslinked nanogels based on HA-m-poly(DAAM-co-DMA) and native HA with Cy5.5

Fluorescent nanogels were obtained by grafting the dye Cy5.5-amine on crosslinked nanogels based on HA-m-poly(DAAM-co-DMA) by an amine-acid coupling reaction using DMTMM as a coupling agent[31]. To this end, crosslinked nanogels (0.010 g, 0.0052 mmol) were solubilized in water/DMF (1:1 v/v; 4 mL) and DMTMM (1.467 mg, 0.0052 mmol) was added to the solution, followed by adjusting the pH to 6.5. After 30 min of stirring, Cy5.5-amine (0.099 mg, 0.00013 mmol) solubilized in water/DMF (1:1 v/v) at a concentration of 1 g/L was added to the reaction mixture. After stirring at room temperature for 48 h, the nanogels were purified by dialysis using a membrane MWCO 6-8 KDa against deionized water for 48 h and recovered by freeze-drying. Cy5.5-labeled HA was prepared from native HA and Cy5.5-amine according to the same procedure.

Scanning electron microscopy

Drops of crosslinked nanogels solutions (0.5 g/L) in pure water at both 5 and 40 °C were deposited onto mica-coated copper stubs (also precooled/heated at 5 or 40 °C, respectively) and allowed to air-drying at 4 or 40 °C. The samples were then coated by approximately 2 nm of sputtered Au-Pd and observed in secondary electron imaging mode with a ZEISS Ultra 55 FEG-SEM (Grenoble INP - CMTC). Images were acquired at low voltage of 3 kV using an in-lens detector.

Cryo-transmission electron microscopy

Cryo-TEM samples were prepared with an automated vitrification system (Vitrobot Mark IV, FEI, The Netherlands). Crosslinked nanogels solutions (5 g/L) was placed on Lacey carbon grids (TedPella Inc, California, USA) charged previously by glow discharge with 15 mA for 10 seconds in air atmosphere to make them hydrophilic (Pelco easiGlow). Specimens were prepared in a controlled environment with the temperature and humidity set to 22 °C for 5 °C sample and 37 °C and 100 % for humidity, respectively, which prevented sample evaporation sample during the preparation. A 3 µL sample droplet was deposited on a 300 mesh lacey carbon-coated cooper grid (Ted Pella). The excess fluid was blotted off to create an ultra-thin layer, which spans the holes of the support film of the solutions, and prepared with blot force of approximately -5, blot wait of 20 seconds and blot time of 3 seconds of waiting time before blotting. The prepared samples were immediately vitrified by propelling the grids into liquid ethane at its freezing point (-184 °C). The vitrified sample grids were transferred under liquid nitrogen by the use of a Gatan (Pleasanton, CA, USA) cryo-holder (Model 626) into a JEOL JEM-1400 plus TEM (Jeol, USA) equipped with FEG and operated at 120 kV acceleration voltage. Microscopy was carried out at -175 °C sample temperature with a defocus range of -2 to -4 µm. Images were acquired using an F-416 CMOS camera (TVIPS, Germany). Sample preparation and data acquisition were performed at the Electron Microscopy Laboratory (LME)/Brazilian Nanotechnology National Laboratory (LNNano).

Cell culture

Cells were obtained from American Type Tissue Culture (ATCC, Maryland), or European Collection of Authenticated Cell Cultures (ECACC). Human cervical cancer cells (HeLa cells) were cultured in DMEM supplemented with 10 % heat-inactivated FBS, 2 mM L-glutamine, and 1 mM sodium pyruvate. Mouse mammary carcinoma cells (TS/A-pc)[32] were cultured in RPMI 1640 glutaMAX™ medium supplemented with 10 % heat-inactivated FBS. The cells were cultured at 37 °C under a humidified atmosphere containing 5 % CO_2. The cells were detached by trypsin and counted under the microscope using a Malassez cell. The cells were then centrifuged (5 min, 200 g) and the pellet was resuspended in appropriate medium or sterile NaCl 0.9% for extemporaneous subcutaneous implant to mice.

Analysis of CD44 receptor expression of cells

To measure expression of the HA-binding receptor CD44 in TS/A-pc and HeLa cells, TS/A-pc and HeLa cells were seeded into a 6-well plate at a density of 5×10^5 cells per well and incubated for 24 h at 37 °C in a humidified atmosphere of 5% CO_2. Cells were trypsinated, counted and washed before incubation for 1 h in 300 µL of PBS containing 10 µL of fluorescein isothiocyanate (FITC)-conjugated mouse anti-human CD44 antibody (#555478 from BD Pharmingen) at 4 °C. FITC mouse IgG2b κ antibody was used as isotype control (# 555742 from BD Pharmingen). After three washing with PBS, the cells were observed using fluorescence-activated cell sorting (FACS) Accuri 6 (Becton, Dickinson and Company, Pont de Claix, France). Cells were gated to exclude cell debris and 10,000 events were recorded in the gate for fluorescence intensity measurement.

***In vitro* enzyme degradation of nanogels**

In the enzymatic biodegradation experiments, several suspensions of crosslinked HA-m-poly(DAAM-co-DMA) nanogels (1 mg/mL) in PBS (pH = 7.4) containing hyaluronidase at different concentrations (20, 40, 60 and 100 U/mL) were incubated at 37 °C. At a

predetermined period, the light scattering intensity, polydispersity index and mean diameter of the samples were measured at 37 °C by DLS.

Cellular uptake of nanogels and *In vitro* cytotoxicity

HeLa and TSA cells were plated in 4-wells Lab-Tek I Chamber slide (Nunc™, Thermo Scientific) (50,000 cells in 500 µL of culture medium) and incubated overnight in DMEM medium at 37 °C and 5% CO_2. Uptake experiments were performed by incubating cells during 4 h, 8 h, and 24 h with Cy5.5-labeled crosslinked nanogels solution (100 µg/mL) at 37 °C and 5 % CO_2. For confocal imaging, cells were fixed in 4% paraformaldehyde for 10 min, and microscopy images were recorded on a Zeiss LMS510 microscope. Images were processed with ImageJ software. Similar protocol was observed for FACS experiment, with a 4 and a 24 h incubation with PBS containing Cy5.5-labeled crosslinked nanogels solution (50 µg/mL). After three washing with PBS, the cells were observed using LSR II (Becton, Dickinson and Company, Pont de Claix, France). Cells were gated to exclude cell debris and 10,000 events were recorded in the gate for fluorescence intensity measurement. For the cytotoxicity assay, HeLa and TSA were seeded at 5 x 10^5 cells/mL in DMEM containing FBS, in 96-well microplates at 37 °C, 5% CO_2 atmosphere. After 24 h, the cells were treated with the crosslinked nanogels and initial HA, at different concentrations. After 72 h of incubation, the cultures were evaluated by MTS assay.

In vivo biodistribution

The *in vivo* behavior of crosslinked nanogels was tested in *nude* mice bearing HeLa or TS/A-pc subcutaneous grafts in their right flank (n = 3/condition). Female NMRI *nude* mice (6–8 weeks, Janvier, Le Genest-Saint-Isle, France) were injected subcutaneously with 1 × 10^6 of cells per mouse. After tumor growth (10-12 days for TS/A-pc and 3 weeks for HeLa), anesthetized mice (isoflurane/oxygen 3.5/4 % for induction and 1.5/2 % thereafter; CSP, Cournon, France) were injected in the tail vein with 100 µL of a dispersion of Cy5.5-labeled crosslinked nanogel (3 g/L in PBS). For comparison, Cy5.5-labeled HA (3 g/L in PBS) was also injected. Fluorescence images were acquired by a back-thinned CCD camera (ORCAII-BT-512G, Hamamatsu, Massy, France) after 30 min, 1 h, 2 h 30, 5 h, 24 h and 48 h of the injection. After the imaging, at 24 h and 48 h, the organs and the blood were collected and imaged. Image display and analysis were performed using Wasabi software (Hamamatsu, Massy, France). Semi-quantitative data were obtained by drawing regions of interest (ROI) around each organ. All procedures and experimental protocols were approved by the ethical committee of Grenoble (France) for the use of animal research.

Results and discussion

Synthesis and characterization of core-crosslinked nanogels

To prepare core-crosslinked nanogels, our approach was to functionalize HA with a thermosensitive ketone-containing copolymer prepared from diacetone acrylamide and *N,N*-dimethylacrylamide as illustrated in Figure 1. DAAM is not only interesting as a crosslinkable group but also as a hydrophobic co-monomer of DMA, which allows to prepare copolymers exhibiting a lower critical solution temperature (LCST) below the body temperature.[26] DAAM and DMA were copolymerized by RAFT polymerization using AIBN as an initiator and 2-(butylthiocarbonothioylthio)propanoic acid as a chain transfer agent (CTA). The molar ratio of monomers:CTA was fixed at 100:1 with a DAAM/DMA feed ratio of 2:1. The kinetic plots proved that, in these reaction conditions,

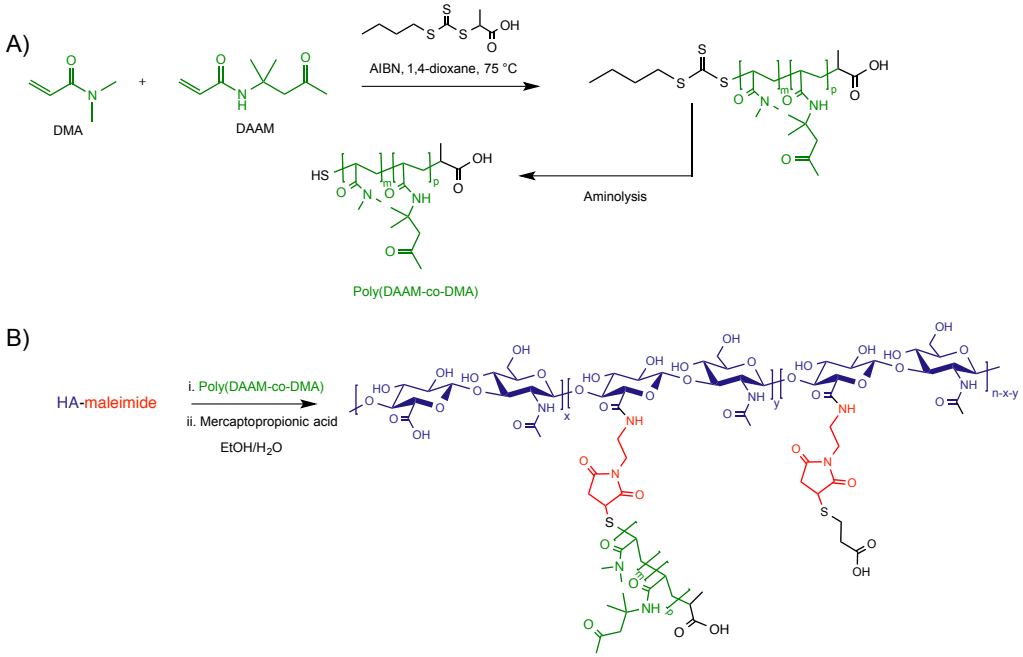

Figure 1. Synthesis of poly(DAAM-co-DMA) and its covalent grafting on hyaluronic acid by a thiol-maleimide coupling reaction.

PABTC allowed a good control over the RAFT copolymerization of DAAM and DMA, resulting in a copolymer with a final DAAM/DMA composition of 57:33 (Figure S1). The resulting copolymer displayed a low dispersity ($Đ$) value (1.11) with a number average molar mass M_n of 16.45 kg/mol. Its structural integrity was ascertained using ^{1}H-NMR analysis (Figure S2). The copolymer exhibited a cloud point temperature of 25.5 °C (Figure S3). Subsequently, poly(DAAM-co-DMA) of which the RAFT trithiocarbonate end-group was converted to a free thiol by aminolysis using *n*-butylamine was grafted onto HA (M_w = 40 kg/mol, namely HA40) containing maleimide moieties (DS = 0.15, derived from ^{1}H NMR analysis) by formation of a thioether bond[29] (Figure 1).

After conversion of the remaining maleimide units to carboxylic acid derivatives by addition of an excess of mercaptopropionic acid, the HA-m-poly(DAAM-co-DMA) conjugate was purified via a batch ion exchange process, and finally dialyzed. The structural integrity of the HA-m-poly(DAAM-co-DMA) was ascertained by ^{1}H NMR analysis. Indeed, comparison of the ^{1}H NMR spectra of initial HA and HA-m-poly(DAAM-co-DMA) shows, for the latter compound, the appearance of new signals in the regions of 3.2-2.1 ppm and 1.7-1.1 ppm, corresponding to the protons of the maleimide-copolymer and maleimide-mecaptopropionic acid adducts, which confirms the successful grafting of the copolymer on HA (Figure 2). The degree of substitution of the conjugate, determined by carbazole assay,[30] was found to be 0.10.

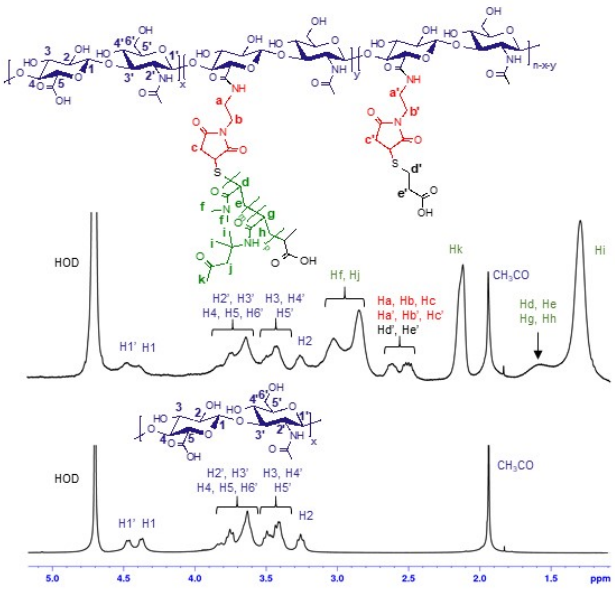

Figure 2. ^{1}H NMR spectrum (400 MHz, 6 g/L in D_2O, 25 °C) of HA-m-poly(DAAM-co-DMA).

HA-m-poly(DAAM-co-DMA) is subjected to a sol-gel transition upon heating in phosphate buffer saline (PBS, pH 7.4) owing to the temperature-responsive behaviour of the grafted copolymer. Nanogels were thus obtained above 32 °C, corresponding to the critical aggregation temperature (CAT) of HA-m-poly(DAAM-co-DMA). This was determined by measuring the light scattering intensity of a solution of the HA derivative in PBS (0.5 g/L) as a function of temperature (Figure S4). The higher value of the CAT compared to the T_{cp} of the copolymer poly(DAAM-co-DMA) can be related to the presence of the highly hydrophilic and negatively charged HA backbone. Dynamic light scattering measurements at 40 °C showed that the nanogels had a hydrodynamic diameter around 145 nm with a low polydispersity index (PDI) of 0.11 (Table 1). The resulting nanogels were subsequently rendered temperature-irreversible by hydrazone-bond crosslinking the keto-functional copolymer chains with a bishydrazide, isophtalic dihydrazide (IDH), in aqueous medium as shown in Scheme 1.

Table 1. Average diameter and PDI of HA-p-poly(DAAM-co-DMA) nanogels.

	18 °C		40 °C	
	Diameter[a] (nm)	PDI	Diameter (nm)[a]	PDI
Non-crosslinked nanogels	–[b]	–[b]	144.6 ± 1.4	0.11
Crosslinked nanogels (0.5 equiv. IDH)	247.1 ± 1.1	0.15	150.6 ± 2.4	0.10

[a] Z-Average diameter; [b] no nanogel formation below the CAT

The cryo-TEM and SEM images of nanogel suspensions vitrified and dried at 5 °C revealed the presence of nanogels at low temperature (Figure 3C and 3E). In accordance to the DLS data (Table 1 and Figure 3B), the nanogels at 40 °C observed by cryo-TEM had a diameter below 200 nm (Figure 3D). The nanogels at 5 °C had a diameter around 200 nm (Figure 3C). This is in line with DLS analysis which indicated an increase of the average diameter of the nanogels from 150 to 247 nm by lowering the temperature from

40 to 18 °C (Table 1). The larger size of the nanogels at 18 and 5 °C can be attributed to increased hydration of the crosslinked copolymer chains, resulting in the nanogel swelling. In the SEM images, the size of the nanogels appeared to be much smaller due to shrinkage during drying.

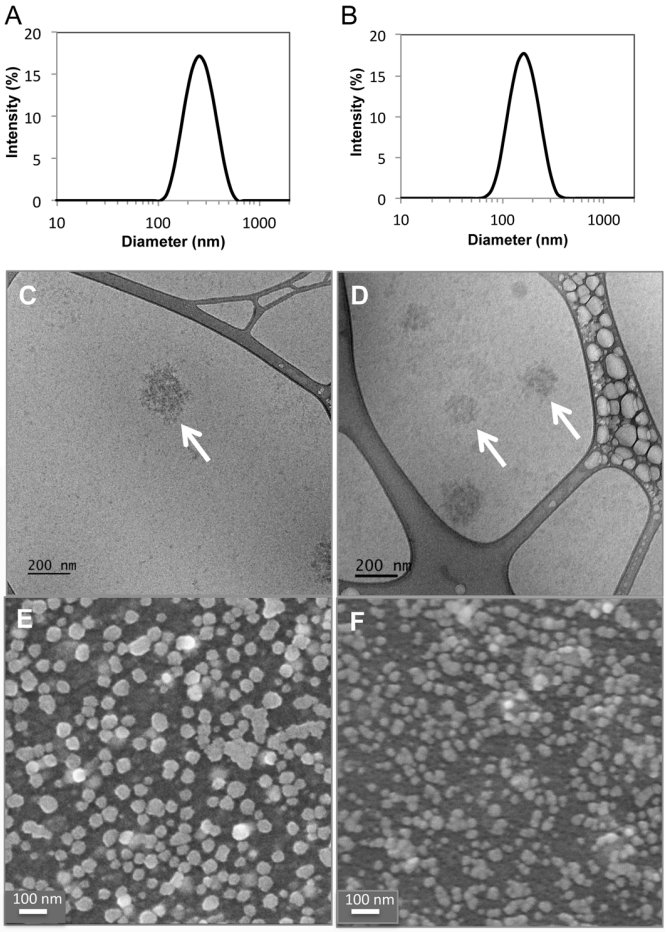

Figure 3. Size distribution of HA-based nanogels crosslinked with an IDH: ketone molar ratio of 0.5 measured by DLS at 18 °C (A) and 40 °C (B); morphology observed at 5 °C (C, E) and 40 °C (D, F) by cryo-TEM (C, D) and SEM (E, F).

In the next step, we varied the IDH to ketone molar ratio from 0.5 to 1.5 in the crosslinking step to ensure that all nanogels were sufficiently crosslinked to be stable at low temperature. The SEM images obtained from crosslinked nanogel suspensions at 5 °C suggested a slightly lower amount of nanogels crosslinked using an IDH to ketone molar ratio of 0.5 (Figure 4A, B and C). This was confirmed by static light scattering experiments performed on the non-crosslinked and crosslinked nanogels (Figure 4D). The non-crosslinked nanogels showed a continuous decrease of the light scattering intensity (LSI) from 40 to 15 °C, indicating gradual disassembly of the nanogels due to hydration of the thermosensitive copolymer chains. The LSI of the nanogels crosslinked with 0.5 molar equiv. of IDH slightly decreased upon cooling, suggesting a small extent of nanogel dissociation. In contrast, the LSI of the nanogels crosslinked with 1 and 1.5 molar equiv. of IDH was constant upon cooling, demonstrating efficient nanogel crosslinking under these conditions.

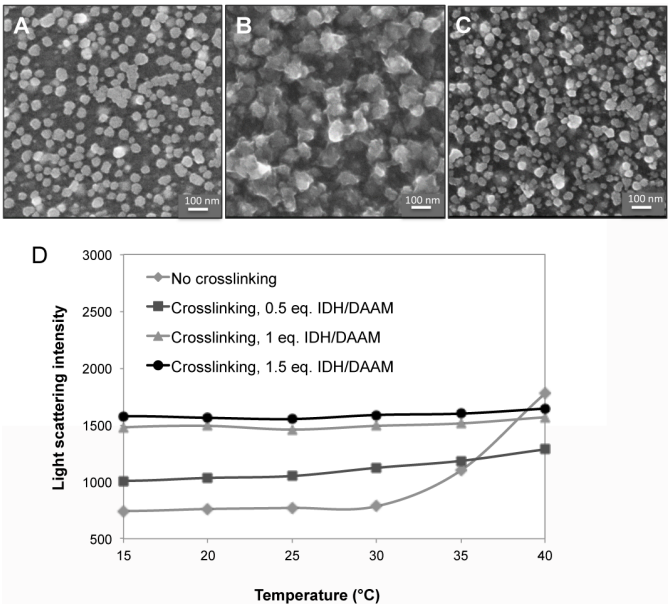

Figure 4. Influence the IDH to ketone molar ratio on the stability of nanogels at low temperature. SEM observation at 5 °C of HA-based nanogels crosslinked with IDH to ketone molar ratios of 0.5 (A), 1.0 (B) and 1.5 (C), and light scattering intensity of non-crosslinked HA-based nanogels and nanogels crosslinked with IDH to ketone molar ratios of 0.5, 1.0 and 1.5 upon cooling from 40 to 15 °C (D).

These results also indicate that the crosslinking density can be tuned by varying the degree of dihydrazide to diacetone monomer molar ratio. Compared to strategies previously used for covalently crosslinking self-assembled nanoparticles based on HA,[16] this approach based on keto-hydrazide chemistry has the advantage of controlling efficiently the extent of crosslinking. As the acylhydrazone can be hydrolyzed under acidic conditions, we evaluated the hydrolytic stability of the cross-linked nanogels at the endosomal pH of 5. We found that at this pH, the nanogels remained stable for prolonged periods of time at 37 °C. We attribute this to the hydrophobic environment within the collapsed copolymer domains. Moreover, in a previous study on macrogels formed by crosslinking poly(DAAM-co-DMA) with adipic acid dihydrazide, the networks were shown to remain stable for several days at pH 6.[22] A pH of 2.5 was required to observe degradation in less than a day. Since HA can be readily degraded to lower molecular weight components by hyaluronidase (HAase) after being taken up by cancer cells,[14] we also investigated the enzymatic degradation of crosslinked nanogels using different concentration of HAase (20, 40, 60 and 100 U/mL) by DLS at 37 °C. The light scattering intensity of the samples was found to rapidly drop, leveling off at 1 h post-addition of HAase. At this time, the LSI was reduced by about 75% and 48 % for HAase concentrations of 20 and 40 U/mL, respectively (Figure S5). Meanwhile, the PDI and the particle size increased to ~ 0.35 and ~ 200 nm, respectively. Further increase of HAase concentration had no significant effect on the LSI and PDI values and the mean size did not change (~ 180 nm). These data suggest partial degradation of nanogels due to the ability of HAase to hydrolyze the outer HA layer of the particles. The evaluation of the biological properties was performed using crosslinked nanogels, which were stable upon long-term storage, as revealed by the perfect solubilization of the product in aqueous solution after freeze-drying. By contrast, non-crosslinked HA-m-poly(DAAM-co-DMA) was not stable enough; this may be due to side reactions involving ketone functional groups though they are more stable than aldehydes. The crosslinking step constitutes therefore an innovative way to stabilize the nanogels.

In vitro cellular uptake evaluation and in vivo targeting properties of nanogels based on HA-m-poly(DAAM-co-DMA)

The intracellular uptake behaviour was observed by confocal microscopy in two cancer cell lines, TS/A-pc (mouse mammary adenocarcinoma) and HeLa (human cervical cancer cells), after 4 h, 8 h, and 24 h incubation with the crosslinked nanogels labeled with Cy5.5. As shown in Figure 5, the time dependent cellular uptake of nanogels was more pronounced in HeLa cells, overexpressing the CD44 receptor for HA than that in TS/A-pc cells which do not express CD44 (see experimental section and supporting information, Figure S6). The internalized nanogels were mainly observed into small vesicles, or diffused in the cytoplasm. This high uptake by HeLa cells was confirmed by FACS experiments, and increased between 4 h and 24 h, as indicated in Figure 5. Such accumulation may be related to the overexpressed CD44 receptor in HeLa cells[33-35], and was safe for both cell lines (see Figure S7). Indeed, CD44 binds HA and enables its internalization and intracellular degradation.[14] In this regard, several studies demonstrated that the degree of intracellular uptake of HA nanoparticles depends on the receptor density of the cells; higher CD44 receptor density correlates with higher HA nanoparticle uptake.[17, 36-38] The *in vivo* biodistribution and tumor accumulation of crosslinked nanogels (with 0.5 equiv. IDH) labeled with Cy5.5 were assessed by non-invasive full body fluorescence imaging following their intravenous administration in HeLa and TS/A-pc tumor-bearing mice, and compared to the biodistribution of Cy5.5-labeled HA. TS/A-pc tumor model was selected in addition to HeLa cell tumor because of its high capacity to accumulate nanoparticles *via* the EPR effect[39].

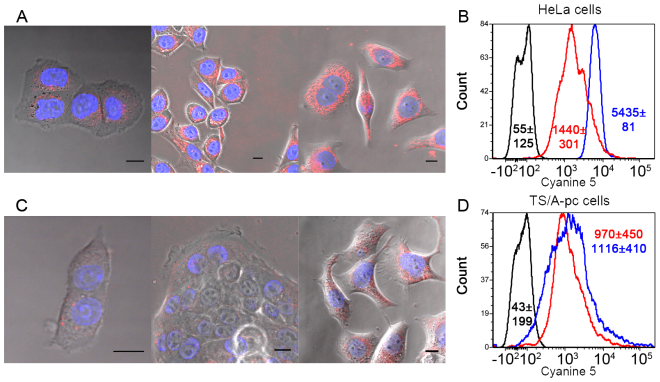

Figure 5. Confocal imaging of HeLa (A) and TS/A-pc (C) cells, 4 h, 8h, and 24 h after incubation with Cy5.5-HA-m-poly(DAAM-co-DMA) crosslinked nanogels. The Cy5.5-labeled crosslinked nanogels are represented by red color, while the cell nuclei are in blue. Scale bar: 10 µm. (B; D) FACS analysis were performed on the same cell lines after 4 h (red line) or 24 h (blue line) and are compared to control condition (Black line).

The fluorescence signal of the crosslinked nanogel was recorded as a function of time in animals, and also in organs after sampling at 24 and 48 h. Fluorescence intensity in the tumor gradually increased up to 24-48 h for both tumor types but to a greater extent in TS/A-pc tumor-bearing mice (Figure 6A). Indeed, TS/A-pc tumors strongly accumulated the nanogels at 24 h with an *ex-vivo* tumor-to-liver ratio reaching ≈ 1 and a tumor-to-muscle ratio reaching ≈ 25 (*versus* ≈ 0.2 and < 3.5, respectively for HeLa tumors, see Figure 6B and C). One should note that these ratios were almost stable between 24 and 48 h. Tumors maintained strong fluorescence intensities during two days as evidenced by quantitative analysis (Figure 6D). This indicated that nanogels could circulate for a long period of time in the body and continuously accumulate at the tumor site. The lower level of accumulation of the nanogels in HeLa as compared to TS/A-pc tumors (Figure 6B and 6C) supports the idea that the capture of nanogels is mostly sensitive to an EPR-driven passive accumulation rather than a CD44-dependent targeted one. This also reflects that passive accumulation of nanoparticles is dependent on the tumor type.[39-41]

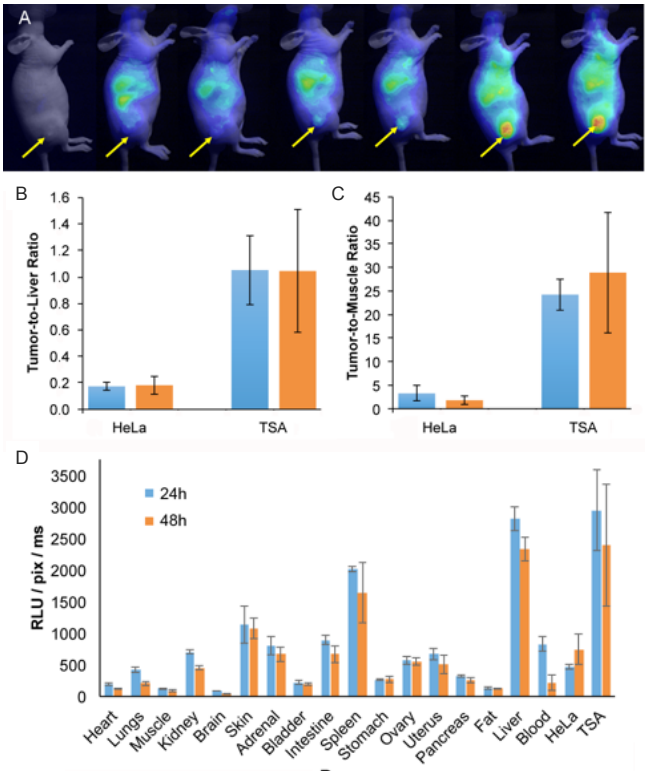

Figure 6. (A) In vivo near-infrared fluorescence (NIRF) images of the time dependent biodistribution of Cy5.5-labeled crosslinked nanogels in breast TS/A-pc and HeLa tumor-bearing mice (n = 3/tumor type). The tumor was engrafted subcutaneously on the right flank of the mouse. The fluorescence was measured at the following time elapse after administration: 0 min, 30 min, 1 h, 2 h 30, 5 h, 24 h, and 48 h. The tumor locations are indicated by the arrows. (B) Fluorescence intensity of the tumor-to-liver ratios at 24 h (blue) and 48 h (orange) post-injection and, (C) tumor-to-muscle ratios from excised organs sampled at 24 h (blue) and 48 h (orange) post-injection. The results are expressed as the mean ± SD (n=3). (D) Quantification of the *ex vivo* biodistribution of Cy5.5-labeled crosslinked nanogels in mice, 24 h and 48 h after administration (n = 6/organ). ROIs were defined on the extracted organs to semi-quantify the amount of photons detected per pixel. The results in each organ are expressed as the mean of relative light unit per pixel per ms ± SD (n=6).

Interestingly, similar results for native HA accumulation were observed as described in Figure S8. Only the tumor-to-muscle ratios were different from the nanogels, reaching 7.18-12.42 for HeLa tumors, and 15.59-8.73 for TS/A-pc tumors, at 24 and 48 h, respectively (Figure S8B and S8C). This highlights the fact that accumulation of nanogels in the tumor is governed by both the nature of their hydrophilic shell and their nanoparticle form. The nanogel fluorescence was also detected in other organs to various extents, with liver and spleen characterized by the highest nanogel accumulations at both 24 and 48 h post injection (Figure 6D). This accumulation may be due to cellular uptake of the nanogels by phagocytic cells of the reticuloendothelial system. It is known that the liver is the major organ that uptakes and accumulates any types of nano/micro particles with high hydrodynamic radius.[42] Accumulation in liver and spleen may also be related to nanogel clearance from circulation mediated by the hyaluronan receptor for endocytosis (HARE), which is found primarily in the sinusoidal endothelial cells of the liver and spleen.[14, 43, 44] Regarding HA, its fluorescence signal was detected with high intensity in liver, spleen as well as in intestine, skin and ovary (Figure S8D). Collectively, these results suggest that crosslinked nanogels exhibit high tumor uptake, probably in correlation with the EPR properties of the tumor, and improved biodistribution even after 48 h post-injection.

Conclusions

In this study, novel biocompatible nanogels were fabricated from hyaluronic acid modified with a ketone-functional copolymer. The nanogels were prepared by a simple method based on the temperature-triggered assembly of the HA conjugate followed by crosslinking the hydrophobic nanodomains of the copolymer chains by hydrazone formation. These crosslinks throughout the hydrophobic domains in the core of the nanogels do not affect the shell-forming polysaccharide structure. In addition, their density can be tuned by varying the dihydrazide crosslinker to ketone group molar ratio. *In vitro* biological studies revealed that the nanogels were internalized into different cell types, with a main vesicle accumulation. Finally, *in vivo* studies demonstrated that following intravenous administration in tumor-bearing mice, the crosslinked nanogels were able to circulate in the bloodstream for a long period of time and accumulated in the tumor tissues, probably in correlation with the EPR properties of the tumor. These results suggest that these nanogels hold great potential in anti-cancer therapy, as they efficiently reach the vascularized tumor. They represent a versatile platform to introduce additional functionalities and/or tune the properties of the hydrophilic shell in order to more optimally exploit the biocompatibility and the beneficial distribution of these novel nanocarriers that might be used for the delivery of chemotherapeutics.

Conflicts of interest

"There are no conflicts to declare".

Acknowledgements

The authors thank the "Conselho Nacional de Desenvolvimento Científico e Tecnológico- Conselho Nacional de Desenvolvimento Científico e Tecnológico (CNPq)" for financial support to this work. F.P.G. gratefully acknowledges the "Science Without Borders Program" of CNPq for the sandwich doctorate scholarship. This work was also partly supported by the "Agence Nationale pour la Recherche" (grant ANR-14-CE08-0014-01 for the "OPENER" project) as well as in the framework of the Glyco@Alps project of the "Investissements d'avenir" program (ANR-15-IDEX-02). This work was also supported through grants from the Capacitação de Aperfeiçoamento de Pessoal de Nível Superior (CAPES) and Financiadora de Estudos e Projetos (FINEP). The authors thank LME/LNNano as well as Dr. Rodrigo Portugal and Dr. Alexandre Cassago for the use of electron microscopy facility and technical support; Francine Roussel-Dherbey at Grenoble INP-CMTC for her help with SEM observations; the NMR platform of ICMG (FR2607) for its support. They gratefully acknowledge O. Stephan at LIphy (Grenoble), who kindly provided DSB.

Notes and references

1. A. Debele Tilahun, L. Mekuria Shewaye and H.-C. Tsai, *Mater Sci Eng C Mater Biol Appl*, 2016, **68**, 964-981.
2. Y. Li, D. Maciel, J. Rodrigues, X. Shi and H. Tomas, *Chem. Rev. (Washington, DC, U. S.)*, 2015, **115**, 8564-8608.
3. G. Soni and S. Yadav Khushwant, *Saudi Pharm J*, 2016, **24**, 133-139.
4. H.-Q. Wu and C.-C. Wang, *Langmuir*, 2016, **32**, 6211-6225.
5. M. M. Yallapu, M. Jaggi and S. C. Chauhan, *Drug Discovery Today*, 2011, **16**, 457-463.
6. Y. H. Bae and H. Yin, *J. Controlled Release*, 2008, **131**, 2-4.
7. H. Maeda, J. Wu, T. Sawa, Y. Matsumura and K. Hori, *J. Controlled Release*, 2000, **65**, 271-284.
8. Y. Matsumura and H. Maeda, *Cancer Res.*, 1986, **46**, 6387-6392.
9. R. K. O'Reilly, C. J. Hawker and K. L. Wooley, *Chem. Soc. Rev.*, 2006, **35**, 1068-1083.

10. E. S. Read and S. P. Armes, *Chem. Commun. (Cambridge, U. K.)*, 2007, DOI: 10.1039/b701217a, 3021-3035.
11. Y. Shao, W. Huang, C. Shi, S. T. Atkinson and J. Luo, *Ther. Delivery*, 2012, **3**, 1409-1427.
12. M. Talelli, M. Barz, C. J. F. Rijcken, F. Kiessling, W. E. Hennink and T. Lammers, *Nano Today*, 2015, **10**, 93-117.
13. C. F. van Nostrum, *Soft Matter*, 2011, **7**, 3246-3259.
14. K. Y. Choi, G. Saravanakumar, J. H. Park and K. Park, *Colloids Surf., B*, 2012, **99**, 82-94.
15. F. Dosio, S. Arpicco, B. Stella and E. Fattal, *Adv. Drug Delivery Rev.*, 2016, **97**, 204-236.
16. N. V. Rao, H. Y. Yoon, H. S. Han, H. Ko, S. Son, M. Lee, H. Lee, D.-G. Jo, Y. M. Kang and J. H. Park, *Expert Opin. Drug Delivery*, 2016, **13**, 239-252.
17. H. S. Han, K. Y. Choi, H. Ko, J. Jeon, G. Saravanakumar, Y. D. Suh, D. S. Lee and J. H. Park, *J. Controlled Release*, 2015, **200**, 158-166.
18. Y. Tao, J. Xu, M. Chen, H. Bai and X. Liu, *Carbohydr. Polym.*, 2012, **88**, 118-124.
19. H. Zheng, L. Yin, X. Zhang, H. Zhang, R. Hu, Y. Yin, T. Qiu, X. Xiong and Q. Wang, *J. Biomed. Nanotechnol.*, 2016, **12**, 1641-1653.
20. Y. Zhong, J. Zhang, R. Cheng, C. Deng, F. Meng, F. Xie and Z. Zhong, *J. Controlled Release*, 2015, **205**, 144-154.
21. Y. Zhu, J. Zhang, F. Meng, L. Cheng, J. Feijen and Z. Zhong, *J. Mater. Chem. B*, 2018, DOI: 10.1039/c8tb00094h, Ahead of Print.
22. Z. Guo, W. Ma, H. Gu, Y. Feng, Z. He, Q. Chen, X. Mao, J. Zhang and L. Zheng, *Soft Matter*, 2017, **13**, 7371-7380.
23. J. Liu, R. C. Li, G. J. Sand, V. Bulmus, T. P. Davis and H. D. Maynard, *Macromolecules (Washington, DC, U. S.)*, 2013, **46**, 8-14.
24. S. Mukherjee, A. P. Bapat, M. R. Hill and B. S. Sumerlin, *Polym. Chem.*, 2014, **5**, 6923-6931.
25. M. Patenaude, S. Campbell, D. Kinio and T. Hoare, *Biomacromolecules*, 2014, **15**, 781-790.
26. X. Tang, J. Han, Z. Zhu, X. Lu, H. Chen and Y. Cai, *Polym. Chem.*, 2014, **5**, 4115-4123.
27. W. Zhou, Q. Qu, Y. Xu and Z. An, *ACS Macro Lett.*, 2015, **4**, 495-499.
28. C. J. Ferguson, R. J. Hughes, D. Nguyen, B. T. T. Pham, R. G. Gilbert, A. K. Serelis, C. H. Such and B. S. Hawkett, *Macromolecules*, 2005, **38**, 2191-2204.
29. J. Jing, D. Alaimo, E. De Vlieghere, C. Jerome, O. De Wever, B. G. De Geest and R. Auzely-Velty, *J. Mater. Chem. B*, 2013, **1**, 3883-3887.
30. M. Cesaretti, E. Luppi, F. Maccari and N. Volpi, *Carbohydr. Polym.*, 2003, **54**, 59-61.
31. M. D'Este, D. Eglin and M. Alini, *Carbohydr. Polym.*, 2014, **108**, 239-246.
32. P. L. Lollini, C. D. Giovanni, L. Landuzzi, G. Nicoletti, F. Frabetti, F. Cavallo, M. Giovarelli, G. Forni, A. Modica and et al., *Hum. Gene Ther.*, 1995, **6**, 743-752.
33. Y. Huang, C. Song, H. Li, R. Zhang, R. Jiang, X. Liu, G. Zhang, Q. Fan, L. Wang and W. Huang, *ACS Appl. Mater. Interfaces*, 2015, **7**, 21529-21537.
34. F. Li, B.-c. Bae and K. Na, *Bioconjugate Chem.*, 2010, **21**, 1312-1320.
35. W. Park, K. s. Kim, B.-c. Bae, Y.-H. Kim and K. Na, *Eur. J. Pharm. Sci.*, 2010, **40**, 367-375.
36. H.-J. Cho, H. Y. Yoon, H. Koo, S.-H. Ko, J.-S. Shim, J.-H. Lee, K. Kim, I. C. Kwon and D.-D. Kim, *Biomaterials*, 2011, **32**, 7181-7190.
37. J. Huang, H. Zhang, Y. Yu, Y. Chen, D. Wang, G. Zhang, G. Zhou, J. Liu, Z. Sun, D. Sun, Y. Lu and Y. Zhong, *Biomaterials*, 2014, **35**, 550-566.
38. H. S. S. Qhattal and X. Liu, *Mol. Pharmaceutics*, 2011, **8**, 1233-1246.
39. A. Karageorgis, S. Dufort, L. Sancey, M. Henry, S. Hirsjarvi, C. Passirani, J.-P. Benoit, J. Gravier, I. Texier, O. Montigon, M. Benmerad, V. Siroux, E. L. Barbier and J.-L. Coll, *Sci. Rep.*, 2016, **6**, 21417.
40. E. Blanco, H. Shen and M. Ferrari, *Nat. Biotechnol.*, 2015, **33**, 941-951.
41. L. Dai, J. Liu, Z. Luo, M. Li and K. Cai, *J. Mater. Chem. B*, 2016, **4**, 6758-6772.
42. J.-Y. Kim, W. I. Choi, Y. H. Kim and G. Tae, *J. Controlled Release*, 2011, **156**, 398-405.
43. E. N. Harris, J. A. Weigel and P. H. Weigel, *J. Biol. Chem.*, 2008, **283**, 17341-17350.
44. M. Zheng, S. Kimura, J. Nio-Kobayashi and T. Iwanaga, *Biomed. Res.*, 2016, **37**, 187-198.